Electron Paramagnetic Resonance and Electron Nuclear Double Resonance Spectroscopic Identification and Characterization of the Tyrosyl Radicals in Prostaglandin H Synthase 1[†]

Wenjun Shi, Curtis W. Hoganson, Matthew Espe,[‡] Christopher J. Bender,[§] and Gerald T. Babcock*

Department of Chemistry, Michigan State University, East Lansing, Michigan 48824

Graham Palmer

Department of Biochemistry and Cell Biology, Rice University, Houston, Texas 77251

Richard J. Kulmacz and Ah-lim Tsai*

Department of Internal Medicine, University of Texas Health Science Center at Houston, Houston, Texas 77225

Received November 5, 1999; Revised Manuscript Received January 24, 2000

ABSTRACT: The tyrosyl radicals generated in reactions of ethyl hydrogen peroxide with both native and indomethacin-pretreated prostaglandin H synthase 1 (PGHS-1) were examined by low-temperature electron paramagnetic resonance (EPR) and electron nuclear double resonance (ENDOR) spectroscopies. In the reaction of peroxide with the native enzyme at 0 °C, the tyrosyl radical EPR signal underwent a continuous reduction in line width and lost intensity as the incubation time increased, changing from an initial, 35-G wide doublet to a wide singlet of slightly smaller line width and finally to a 25-G narrow singlet. The 25-G narrow singlet produced by self-inactivation was distinctly broader than the 22-G narrow singlet obtained by indomethacin treatment. Analysis of the narrow singlet EPR spectra of self-inactivated and indomethacin-pretreated enzymes suggests that they reflect conformationally distinct tyrosyl radicals. ENDOR spectroscopy allowed more detailed characterization by providing hyperfine couplings for ring and methylene protons. These results establish that the wide doublet and the 22-G narrow singlet EPR signals arise from tyrosyl radicals with different side-chain conformations. The wide-singlet ENDOR spectrum, however, is best accounted for as a mixture of native wide-doublet and self-inactivated 25-G narrow-singlet species, consistent with an earlier EPR study [DeGray et al. (1992) *J. Biol. Chem. 267*, 23583−23588]. We conclude that a tyrosyl residue other than the catalytically essential Y385 species is most likely responsible for the indomethacin-inhibited, narrow-singlet spectrum. Thus, this inhibitor may function by redirecting radical formation to a catalytically inactive side chain. Either radical migration or conformational relaxation at Y385 produces the 25-G narrow singlet during self-inactivation. Our ENDOR data also indicate that the catalytically active, wide-doublet species is not hydrogen bonded, which may enhance its reactivity toward the fatty-acid substrate bound nearby.

The two isoforms of prostaglandin H synthase (PGHS)[1], PGHS-1 and PGHS-2, are integral membrane hemoproteins that catalyze the first steps in the biosynthesis of prostaglandins (PGs) and thromboxane from fatty acids (for review, see refs *1* and *2*). Both PGHS isoforms have two distinct catalytic activities, as illustrated:

$$\text{arachidonic acid} \xrightarrow{\text{cyclooxygenase}} PGG_2 \xrightarrow{\text{peroxidase}} PGH_2 \quad (1)$$

The mechanism proposed for PGHS cyclooxygenase activity involves an initial abstraction of hydrogen from C13 of the fatty acid to form a radical, followed by reaction with two oxygen molecules and cyclization to form PGG_2 (*3*). Formation of arachidonate radicals in the cyclooxygenase reaction has been demonstrated indirectly by spin-trapping experiments with PGHS-1 (*4*) and by direct EPR observations of both isoforms (*5, 6*).

At least four organic-radical EPR signals, with distinct line shapes, have been detected in PGHS-1 reactions. Addition of arachidonate or hydroperoxides to native PGHS-1 initially produces a doublet EPR signal with a peak-to-trough line width of 33−35 G (*7, 8*). Upon further incubation, this EPR signal, customarily called the wide doublet for its characteristic line shape, undergoes a transition to a singlet with approximately the same line width. This latter spectrum is referred to as a wide singlet, and it persists for many minutes at 0 °C. Two singlet-like EPR species, with much narrower line widths, are observed either at a much later stage of the reaction (line width ∼ 26 G) (*9*) or when the enzyme is pretreated with cyclooxygenase inhibitors such as aspirin or

[†] This research was supported by NIH Grants GM57323 and GM37300 to G.T.B., GM30509 and GM52170 to R.J.K., GM21337 to G.P., and GM44911 to A.-l.T.

* Corresponding authors: G.T.B.: e-mail babcock@cem.msu.edu; telephone 517-355-9715; fax, 517-353-1793. A.-l.T.: e-mail atsai@heart.med.uth.tmc.edu; telephone 713-500-6771; fax 713-500-6810.

[‡] Present address: Department of Chemistry, University of Akron, Akron, OH 44325.

[§] Present address: Department of Chemistry, Fordham University, Bronx, NY 10458.

[1] Abbreviations: ENDOR, electron nuclear double resonance; EPR, electron paramagnetic resonance; EtOOH, ethyl hydroperoxide; PG, prostaglandin; PGHS, prostaglandin synthase 1.

10.1021/bi992561c CCC: $19.00
Published on Web 03/16/2000

indomethacin (line width ~ 22 G) (*10*). These spectra are often referred to as narrow-singlet signals. Experiments with PGHS-1 containing deuterated tyrosine have demonstrated that the hydroperoxide-induced radicals are all tyrosyl radicals (*11*). Other evidence indicates that similar radicals in PGHS-2 are also tyrosyl radicals (*12*−*14*).

The possible role of tyrosyl radicals in PGHS catalytic activity has been under intensive study. There is evidence that the cyclooxygenase activity occurs through a peroxide-initiated free radical mechanism and that the wide-doublet tyrosyl EPR signal is present during cyclooxygenase catalysis (*7*, *8*, *10*). Chemical modification and site-directed mutagenesis studies have demonstrated that a specific tyrosine residue in PGHS-1, Y385, is essential for cyclooxygenase activity and for generation of the wide-doublet signal (*11*, *15*). Results from single-turnover experiments have provided direct evidence that the wide-doublet tyrosyl radical, generated in the peroxidase cycle, can oxidize the cyclooxygenase substrate, arachidonic acid, to a fatty acyl radical (*5*, *6*). It is, therefore, clear that the wide doublet tyrosyl radical has a functional role in cyclooxygenase catalysis. In contrast, the narrow-singlet species that is observed with enzyme complexed with indomethacin does not oxidize arachidonic acid and is ineffective in normal cyclooxygenase activity (*5*). The catalytic importance of the wide-singlet species is unclear. Although it is able to oxidize arachidonic acid (*5*), accumulation of the wide singlet lags the production of PGG_2/PGH_2 (*16*, *17*).

A closely related issue is the number of structurally distinct radical species involved. Lassman et al. (*16*) and Degray et al. (*9*) observed the wide-doublet, the wide-singlet, and the 26-G narrow-singlet tyrosyl EPR signals sequentially in the reaction of the native enzyme. Using computer simulation, DeGray et al. (*9*) concluded that the wide singlet is a composite of the wide doublet and the 26-G narrow singlet. However, the relationship between the two narrow-singlet signals, the 26-G radical obtained in the native enzyme and the 22-G signal obtained with the indomethacin-treated enzyme, was not discussed. Kulmacz et al. (*10*) and Tsai et al. (*17*) have reported that narrow-singlet signals were observable both in indomethacin-pretreated enzyme and in the reaction between concentrated PGHS-1 and a large excess of arachidonate, without detectable accumulation of either wide-doublet or wide-singlet tyrosyl radicals. They concluded that the three types of signals represent distinct tyrosyl-radical species.

The previous assignments of tyrosyl-radical species in PGHS-1 were based almost exclusively on analysis of line widths and line shapes of the radical EPR signals. The conclusions from these studies are potentially ambiguous, because anisotropic line-broadening effects on the EPR spectra prevent an accurate determination of the hyperfine structure of each species. To address these issues more directly, we have conducted a detailed study of native PGHS-1 during reaction with substrate peroxides. A 25-G narrow-singlet radical, which displays an EPR line shape different than that of the 22-G narrow singlet of inhibitor-treated enzyme, is obtained in the final stages of the substrate inactivation process. We present results from a proton ENDOR investigation of the wide doublet, wide singlet, and the 22-G narrow singlet to identify and characterize these three tyrosyl-radical species. Analysis of the spectroscopic results shows that the wide singlet is not a distinct species but is rather a sum of varying contributions from the native wide doublet and the reaction-inactivated, narrow singlet. Moreover, we find that the two narrow-singlet species, the reaction-inactivated radical and the indomethacin-inhibited radical, differ conformationally.

MATERIALS AND METHODS

(1) Sample Preparation. Ethyl hydroperoxide (EtOOH) was purchased from Polyscience Inc. (Warrington, PA). Indomethacin and hemin were obtained from Sigma. Arachidonic acid was purchased from NuChek Preps (Elysian, MN). PGHS-1 was purified to electrophoretic homogeneity from sheep seminal vesicles, as described previously (*7*). The holoenzyme was reconstituted with heme, excess heme was removed by DE-52 adsorption, and the holoenzyme was stored at −70 °C with 30% glycerol as cryoprotectant (*7*). Samples with cyclooxygenase activity ranging from 40 to 90 μmol of O_2 min^{-1} mg^{-1} were diluted 3-fold with 50 mM potassium phosphate, pH 7.4, containing 0.02% octyl β-D-glucoside (with or without preincubation with equimolar indomethacin at 4 °C for 1 h) and concentrated to >150 μM (heme concentration) in an Amicon concentrator with a YM-30 membrane. After addition of glycerol to 25−30%, samples were transferred to EPR tubes. H_2O/D_2O solvent exchange was carried out by concentrating 5 mL of the enzyme (~10 μM) in 50 mM phosphate/ 0.02% octyl β-D-glucoside to 300 μL by ultrafiltration. Eight milliliters of 50 mM phosphote/0.02% octyl β-D-glucoside in D_2O was then added and the solution was incubated for 14−16 h at 8 °C. For the indomethacin treatment, the inhibitor was then added at 1:1 stoichiometry and incubated for an additional 30 min. The samples were then concentrated to 200 μL, deuterated glycerol was added to 30%, and the samples were transferred to EPR tubes for subsequent measurements.

(2) Spectroscopies. Preliminary EPR measurements were made with a Varian E6 spectrometer equipped with liquid-helium and liquid-nitrogen transfer systems, as described (*17*). Each sample was reacted at 0 °C with a 5−10-fold excess of EtOOH and freeze-trapped in acetone/dry ice. Spin concentrations were quantified by using a cupric sulfate standard (*11*). The wide-doublet tyrosyl-radical sample was obtained by freeze-trapping at the earliest time point available manually (~5 s). The wide-singlet and narrow-singlet samples were prepared by thawing−freezing cycles until the desired EPR spectral type was obtained. These samples were stored in liquid nitrogen for further spectroscopic characterization.

Detailed EPR spectra were recorded at −155 °C on a Bruker ER-200D X-band spectrometer equipped with a TE_{102} cavity. The modulation frequency was 100 kHz, and the modulation amplitude was 1.5 G. The instrument was also used in conjunction with a Bruker ER-250 ENDOR accessory and an ER-250ENB TM_{100} cavity for conventional frequency-modulated ENDOR spectroscopy. A custom-built helical ENDOR 18-turn coil, similar in design to those described by Hurst et al. (*18*) and by Bender et al. (*19*) was used. Radio frequency power was provided by an ENI 3100L amplifier driven at frequencies generated by a Wavetek Model 3000-446 frequency synthesizer. Because the radical concentrations were relatively low (typically 30−70 μM), two fast-scan

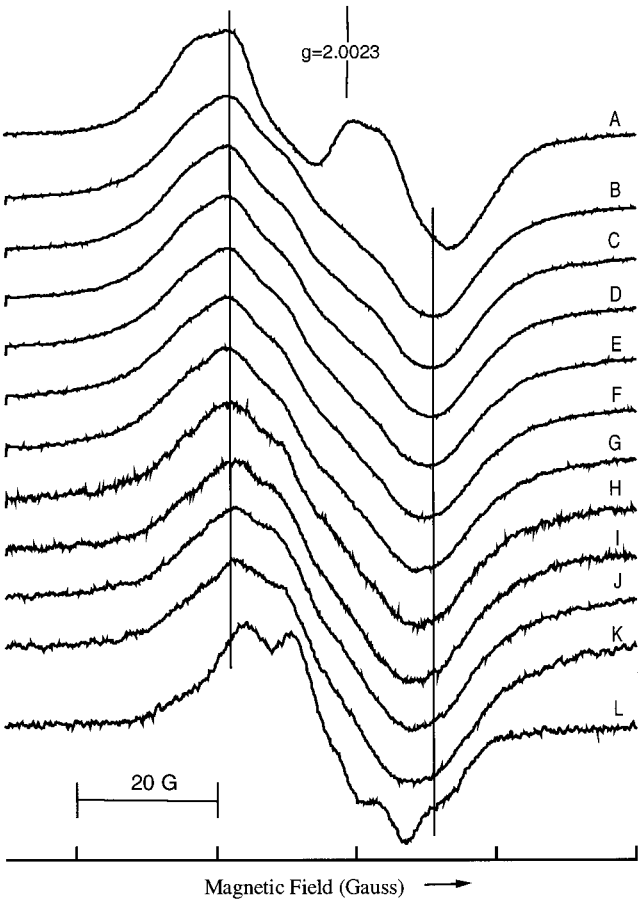

FIGURE 1: Selected EPR traces (spectra A−K) during reaction of native PGHS-1 (213 μM heme) with 5 equiv of EtOOH. Spectrum A was recorded after reaction for 5 s at 0 °C. Thaw/freeze cycles were used subsequently to achieve cumulative reaction times (in minutes), as follows: B, 0.25; C, 0.5; D, 3; E, 10; F, 24; G, 67; H, 181; I, 280; J, 310; and K, 376. Spectrum L is the narrow-singlet signal observed in indomethacin-treated enzyme (200 μM heme) reacted with 5 equiv of EtOOH for 7 s at 0 °C. EPR conditions: for spectrum A, microwave power = 1 mW, modulation amplitude = 2 G, and temperature = 95 K; for spectra B−L, microwave power = 0.2 mW, modulation amplitude = 1.5 G, and temperature = 115 K. All spectra have been center-aligned for easier comparison.

ENDOR methods (transient and rapid-passage ENDOR) were employed to detect the signals from strongly coupled protons. The custom-built transient ENDOR apparatus and procedural details are described elsewhere (*20*). Briefly, a transient ENDOR signal is induced by a pulsed radio frequency magnetic field and is captured by a gated integrator. The rapid-passage ENDOR, operating in dispersion mode, is similar to published designs (*21*, *22*). Precise measurements of microwave frequencies and magnetic-field strengths were made by using a Hewlett-Packard 5255A/5245L frequency converter/counter and a Bruker ER-035M gaussmeter, respectively. All ENDOR experiments were performed at a temperature of approximately 4.2 K, which was maintained with an Oxford ESR900 liquid-helium flow cryostat.

RESULTS

(1) EPR Kinetics Study. EPR spectroscopy was used to monitor tyrosyl-radical signals as a function of time after EtOOH addition to native PGHS. Spectrum A in Figure 1 is from a sample that was trapped at a reaction time of ~5 s and shows the initial wide-doublet tyrosyl-radical signal

Scheme 1

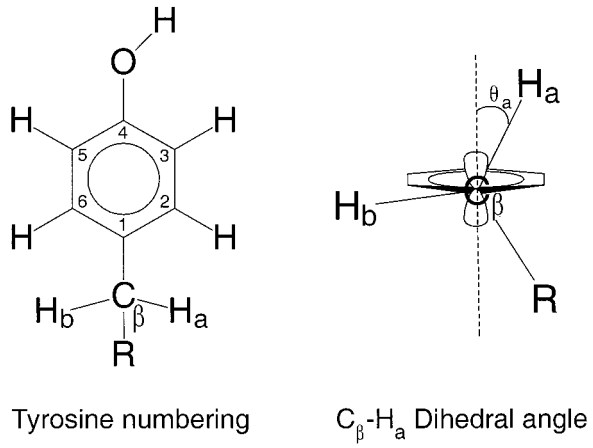

centered at $g = 2.005$ (splitting of ~ 20 G; overall line width of ~ 33 G). The doublet quickly gave way to a singlet with a slightly narrower line width, as shown in spectrum B. A further reduction in line width of the wide-singlet EPR signal is observed upon prolonged incubation of the native enzyme with peroxide, as shown by spectra C−K in Figure 1, which confirms the report by DeGray et al. (*9*). The EPR signal underwent a continuous change in line width from the wide doublet through the wide singlet to a narrow singlet (Figure 1). The narrow-singlet signal (25 G) in our final EtOOH reaction sample, which we designate the reaction-inactivated narrow singlet (spectrum K in Figure 1), is somewhat narrower than the 26-G singlet reported earlier (*9*), presumably because the reaction was allowed to continue longer in the present study. The line shape of the 25 G signal generally resembles the narrow-singlet signal produced in the EtOOH reaction of the inhibitor-pretreated enzyme, but the latter, which we designate the inhibited narrow singlet, has a narrower line width, 22 G (spectrum L in Figure 1), and forms without earlier accumulation of a doublet radical (*7*, *10*).

(2) Simulations of EPR Spectra. There are two plausible explanations for the wide-singlet signals of variable line width observed in Figure 1, as follows: (a) the wide singlets represent distinct tyrosyl-radical species that are generated by, for example, continuous variation in the dihedral angle between the phenol ring carbon and the protons bonded to the β-methylene carbon (Scheme 1); or (b) only the wide doublet and the reaction-inactivated narrow singlet represent distinct tyrosyl-radical species with well-defined conformations, with the wide singlets comprising variable mixtures of the two. DeGray et al. (*9*) provided evidence for the second explanation, as they reproduced the wide-singlet spectra with a simple weighted sum of the 26-G narrow singlet and the initial wide-doublet spectra.

In Figure 2, we consider these possibilities. The EPR spectra of the wide doublet and the inhibited narrow singlet, which are indisputably discrete species, were simulated (Figure 2A,B), and their **g** and **A** tensor components are summarized in Table 1. The experimental wide-singlet spectrum is shown in Figure 2C. A simulation was carried out with the assumption that the wide-singlet spectrum arises from a discrete species (Figure 2C, sim). The **g** and **A** tensor components obtained from this simulation are given in Table 1. The assigned hyperfine coupling constants for the ring protons are essentially identical to those for tyrosyl radicals

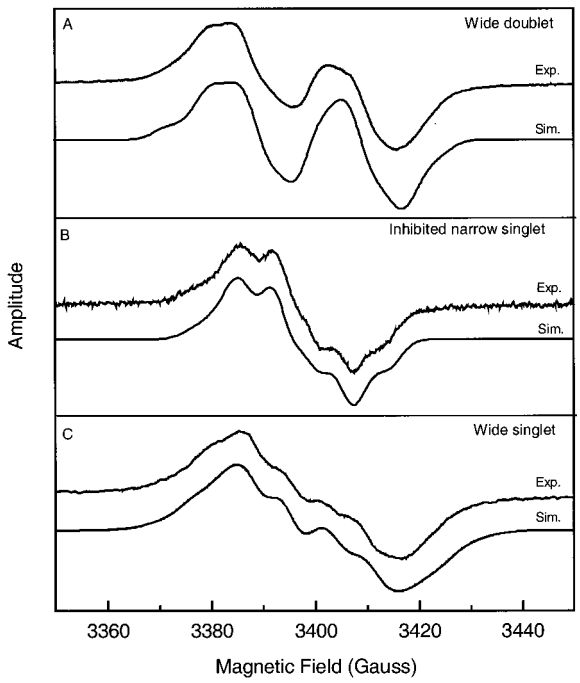

FIGURE 2: X-band and simulated EPR spectra of tyrosyl free radicals produced during reaction of PGHS-1 with 10 equiv of EtOOH at 0 °C. (A) Radical trapped at reaction time of 5 s with native enzyme (159 μM heme). (B) Same as spectrum L of Figure 1. (C) Radical trapped after 27 s of reaction of the native enzyme (164 μM heme) with 10 equiv of EtOOH. Spectra labeled exp are experimental spectra; those labeled Sim are simulated by using the parameters in Table 1. Spectrometer conditions: microwave frequency = 9.5 GHz, microwave power = 0.2 mW, modulation amplitude = 1.5 G, and temperature = 118 K.

Table 1: Best-Fit Parameters of Tyrosyl-Radical EPR Signals in PGH Synthase

parameters	component	wide doublet	wide singlet	narrow singlet
g-tensor	g_x	2.0089	2.0064	2.0074
	g_y	2.0044	2.0044	2.0044
	g_z	2.0023	2.0023	2.0023
3,5-ring protons	A_x[a]	25.7	25.7	25.7
	A_y	7.4	7.5	7.8
	A_x	19.5	19.5	20.9
methylene proton (C_β-H_a)	$A_\perp$	58.2	45.0	27.0
	$A_\parallel$	61.6	50.0	33.0

[a] Absolute values for *A* components are given in megahertz.

in other radical enzymes (*23*). The hyperfine coupling constants for the strongly coupled methylene protons in the simulated wide-singlet spectrum also have values within the limits experimentally determined for other tyrosyl radicals (*23*, *24*). Thus, a reasonable simulation of the PGHS-1 wide-singlet spectrum can be achieved within the context of the first explanation above. We also found, however, that we could reproduce the wide-singlet EPR spectrum reasonably well by taking a weighted sum of wide-doublet and narrow-singlet spectra, as suggested by DeGray et al. (*9*). These results indicate that a more definitive approach than EPR spectral simulation is needed to decide between the two plausible explanations for the wide-singlet spectrum. Double-resonance spectroscopy has the potential to do this, as the EPR parameters in Table 1 for a discrete wide-singlet species predict the presence of specific resonances in the ENDOR spectra.

(3) ENDOR Study. (A) Strongly Coupled Methylene Protons and the Identity of the Wide-Singlet EPR Signal. Previous ENDOR studies on model and protein tyrosyl radicals have shown that resonances from β-methylene protons that are strongly coupled to unpaired electron-spin density in the phenol ring can be detected in the 20−50 MHz radio frequency range at X-band frequencies (*19*, *23*, *24*, *26*, *27*) (see Scheme 1 for the tyrosyl-ring numbering scheme). Because the β-proton couplings are sensitive to the C1−C_β−$H_{a,b}$ dihedral angles (Scheme 1 and ref *28*), this frequency region is useful in detecting tyrosyl-radical conformational differences in PGHS-1. For the four tyrosyl EPR signals observed in reactions of PGHS-1 and indomethacin-treated PGHS-1 with EtOOH, the line width of the wide singlet is narrower than that of the wide doublet but wider than those of the two narrow singlets. This difference in line width is reflected in the EPR simulations in Table 1. Thus, if the wide singlet originates from a conformationally distinct species, the ENDOR peaks due to the methylene protons in this conformation are expected to lie between the ENDOR signals of the wide-doublet and narrow-singlet species. Alternatively, if the wide-singlet EPR signal is a mixture of the wide-doublet and the narrow-singlet signals, then its methylene proton ENDOR signals will be a composite of those of the two contributing species. Thus, a comparison of the ENDOR spectrum of the wide-singlet species with those of the wide-doublet and the two narrow-singlet species should distinguish the two possibilities above for the origin of the wide-singlet species.

The frequency-modulated (FM) ENDOR spectrum of the wide-doublet sample in the 20−45 MHz region is shown in Figure 3. The inset shows the corresponding EPR signal, with an arrow indicating the field at which the ENDOR spectrum was recorded. The features designated as g and h in the ENDOR spectrum are centered around 43 MHz and comprise an axial line shape, although the signal-to-noise ratio in this frequency region of the conventional continuous-wave spectrum is poor. The axial character was confirmed by other ENDOR experiments presented below. The appearance of signals g and h, as well as e (24 MHz) and f (27 MHz) resemble those of the tyrosyl radicals found in ribonucleotide reductase (*19*) and photosystem II (*24*, *27*, *29*). Conventional FM-ENDOR spectroscopy failed to detect signals in the 20−45 MHz radio frequency range for the reaction-inactivated or the inhibited narrow-singlet samples or for the wide singlet, owing to the lower radical concentrations that were trapped.

To improve the signal-to-noise ratio, we employed two fast-scan ENDOR techniques. One is the transient ENDOR developed recently (*20*), and the other is a rapid-passage ENDOR approach. Figure 4A displays the transient-ENDOR spectrum of the wide-doublet radical species. Two peaks, centered at 24 (e) and 27 (f) MHz, are apparent in the 20−30 MHz region. The first derivative of this spectrum (not shown) reveals that the line shape in the 20−30 MHz region is analogous to that in the FM-ENDOR experiment of Figure 3. The peaks at e and f in Figure 4A are assigned to ring protons (see below). Also evident are ENDOR signals centered at 44 MHz (g and h), which together comprise a well-defined axial line shape and are assigned to the strongly coupled β-methylene protons. This assignment is consistent with the general expectation that the hyperfine couplings of

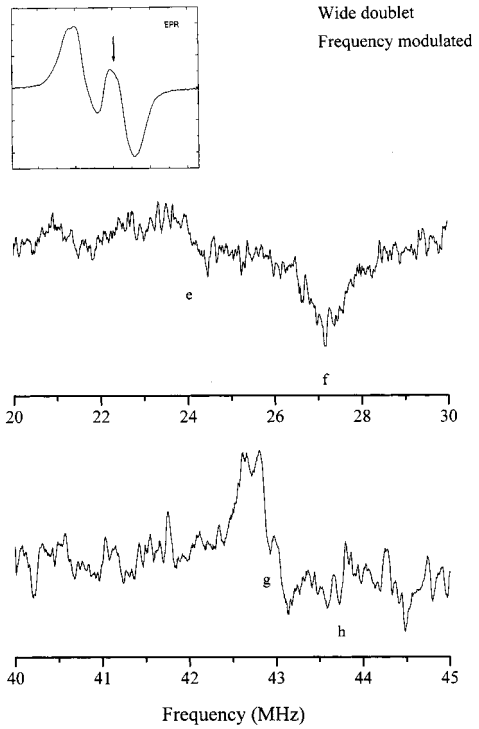

FIGURE 3: X-band, frequency-modulated ENDOR spectra of the wide-doublet radical species (same sample as for the EPR spectrum in Figure 2A). Spectrometer conditions: microwave frequency = 9.4 GHz; microwave power = 2 mW, magnetic field = 3348 G, rf power = 80 W at 10 MHz for the 2−30 MHz portion and 70 W at 20 MHz for the 40−95 MHz portion of the spectrum, and rf modulation = 100 kHz (20−30 MHz) or 150 kHz (40−45 MHz). The corresponding EPR spectrum is shown in the inset.

the methylene protons should be close to axial, as is the case for tyrosyl radicals in ribonucleotide reductase (*19*), galactose oxidase (*26*), and photosystem II (*24*, *27*, *29*). From the g and h turning points, apparent in Figure 4A, we calculated axial tensor components of $A_{\perp} = 58$ MHz and $A_{||} = 62$ MHz for the strongly coupled β-proton in the wide-doublet species (Table 2). Moreover, both the ring α-protons and the strongly coupled β-methylene proton resonances are sharp and well defined, which indicates that there is little dihedral angle dispersion in the tyrosyl radical that gives rise to the wide doublet (*29*−*32*). The wide-doublet spectrum, obtained by using the rapid-passage dispersion ENDOR technique (Figure 4B), is essentially identical to the transient spectrum in Figure 4A, indicating that the two detection methods yield consistent results.

The reaction-inactivated narrow-singlet species was prominent only after long reaction times, when the signal intensity was too small for ENDOR measurements (Figure 1). The inhibited narrow singlet could be prepared in much higher concentrations, however, and was used for ENDOR. Owing to the overall similarity in EPR line shape (*7*, *16*, *17*), the ENDOR properties of the inhibited narrow singlet are likely to resemble those of the reaction-inactivated narrow singlet. The dispersion ENDOR spectrum of the inhibited narrow-singlet sample in the 20−60 MHz frequency region, shown in Figure 4D, lacks the 44 MHz peak observed for the wide-doublet sample; moreover, the high-frequency tail of the 27 MHz peak is more prominent (see below), and the low-frequency shoulder on the 24 MHz peak is more intense.

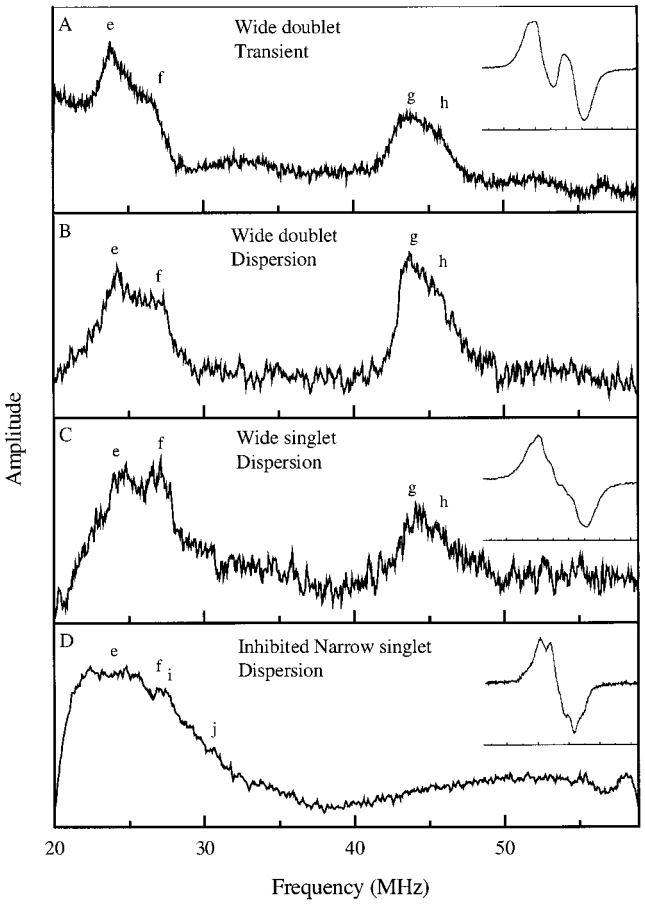

FIGURE 4: Transient and dispersion ENDOR spectra of PGHS-1 radicals. Insets show the corresponding EPR spectra. (A) X-band transient-ENDOR spectrum of the wide-doublet species (same sample as for the EPR spectrum in Figure 2A). Spectrometer conditions: microwave frequency = 9.4 GHz, microwave power = 0.6 mW, scan step = 50 kHz; 6000 scans. (B−D) X-band, rapid-passage, dispersion ENDOR spectra of three PGHS-1 radical samples (same samples as for the EPR studies in Figure 2): (B) wide doublet, (C) wide singlet, and (D) inhibited narrow singlet. Spectrometer conditions: microwave frequency = 9.4 GHz, microwave power = 2 mW, magnetic field = 3341 G, field modulation amplitude = 2.0 G, scan step = 50 kHz; 600 (B), 10 000 (C), or 20 000 (D) scans.

The dispersion ENDOR spectrum of the wide-singlet sample is shown in Figure 4C. This spectrum provides a good test of the two explanations for the origin of the radical. If the wide singlet arises from a discrete species, then the EPR spectral simulation parameters in Table 1 predict ENDOR resonances near 27.5, 24.5, and 18.5 MHz for the 3,5-ring protons and near 39.7 and 37.2 MHz for the strongly coupled β-protons. These latter resonances, however, are not evident in the ENDOR spectrum (Figure 4C). Alternatively, if the wide singlet is a composite spectrum, then resonances of the wide doublet and the narrow singlet should be apparent in its ENDOR spectrum. The features characteristic of the wide doublet at 24 (e), 27 (f), 44 (g), and 46 (h) MHz are clearly seen in the dispersion-detected experimental spectrum from the wide singlet (Figure 4C), with no discrete resonances in the 35−40 MHz region. The amplitude of the peak centered at 44 MHz is smaller than those at 24 and 27 MHz, in contrast to the wide-doublet spectrum, where the relative intensities of the 44 and 46 MHz features and those at 24 and 27 MHz are comparable (Figure 4B). This suggests that

Table 2: Proton Hyperfine Coupling Constants Estimated by Different ENDOR Methods

	wide doublet				narrow singlet			
peak	FM[a]	trans[b]	disp[c]	A[d]	FM	disp	A	assignment[e]
a					15.9		3.1	H-bond
b	16.0			3.5	16.3		3.9	$H_b(A_y)$
c	16.8			4.9	16.8		4.9	2,6-H (A_1)
d	17.9			7.1	18.2		7.5	2,6-H (A_2)
e	24.0	23.8	24.2	19.5		24.7	20.9	3,5-H (A_z)
f	27.1	27.0	27.2	25.7		27.1	25.7	3,5-H (A_x)
g	43.0	43.5	43.7	58.2				H_a ($A_\perp$)
h		45.7	45.9	61.6				H_a ($A_\parallel$)
i						27.8	27.0	H_a ($A_\perp$)
j						30.8	33.0	H_a ($A_\parallel$)

[a] Conventional continuous-wave, frequency-modulated ENDOR; absolute X-band, ENDOR frequency. [b] Transient ENDOR; absolute X-band, ENDOR frequency. [c] Rapid-passage ENDOR operated in dispersion mode; absolute X-band, ENDOR frequency. [d] Hyperfine coupling constants, A, are presented as absolute values in megahertz. [e] Proton and corresponding hyperfine tensor component assignments.

some of the intensity in the 25 MHz region in Figure 4C comes from a species that does not contribute at 44 MHz. In addition, two other features in the wide-singlet spectrum are noticeably different from the wide-doublet ENDOR spectrum. First, there is a long tail on the high-frequency side of peak f; second, a weak shoulder appears on the low-frequency side of peak e. Features in this region are present in the ENDOR of the narrow singlet (Figure 4D) and make the ENDOR spectrum of the wide singlet broader in the 20−30 MHz region than that of the wide doublet.

Thus, there are no features in the wide-singlet ENDOR spectrum that distinguish it from the wide-doublet and the narrow-singlet spectra (Figure 4). This comparison offers direct evidence that the observed EPR signal with a wide-singlet line shape does not originate from a distinct tyrosyl-radical species. Rather, it is clearly consistent with the wide singlet being a mixture of the signals from two distinct tyrosyl radicals that show wide-doublet and narrow-singlet EPR line shapes.

(B) 3,5-Ring Protons. An extensive series of EPR, ENDOR, and electron spin−echo measurements have shown that the spin-density distribution in neutral tyrosyl radicals is essentially constant and insensitive to the local environment near the radical site (*23*, *24*, *27*, *29*, *30*, *33*−*35*). The line width and line shape variations that do occur in this class of radicals are primarily attributable to variations in the dihedral angle between the normal to the phenyl ring and the bond to the methylene proton (Scheme 1). The similarities between the EPR and ENDOR spectra of the PGHS-1 wide-doublet and narrow-singlet signals and those of tyrosyl radicals in ribonucleotide reductase and photosystem II provide a basis for a straightforward assignment of the resolved PGHS ENDOR signals. Accordingly, the signals at 24 (e) and 27 (f) MHz in the dispersion ENDOR spectrum of the wide-doublet sample (Figures 3 and 4) can be assigned to two of the hyperfine tensor components of the 3,5-ring protons.

For the inhibited PGHS-1 narrow-singlet species, the broad features in the 20−35 MHz region in the dispersion ENDOR spectrum (Figure 4D) make determination of corresponding proton hyperfine splittings more difficult. To proceed, we draw on the general behavior of tyrosyl radicals to assign the signals at 24 and 27 MHz, which are just apparent above the broad background and also present in the wide-doublet spectrum, to the 3,5-ring protons. The broad, underlying feature of the ENDOR spectrum in the 20−35 MHz region then can be assigned to a methylene proton. This assumption is consistent with the very similar, long-tailed feature that overlaps sharp signals in the ENDOR spectra of model tyrosyl radicals (*31*, *32*) and of the $Y_Z^\bullet$ radical in manganese-depleted photosystem II preparations (*29*). The spectral broadening in this region, which was assigned to the methylene protons in the model tyrosine species and in $Y_Z^\bullet$ from isotopic substitution experiments, reflects orientational disorder in the methylene-group dihedral angle. The orientational disorder produces a less-resolved line shape in the ENDOR spectrum, compared to signals from tyrosine residues whose geometries are constrained by the surrounding polypeptide (*31*, *32*).

The assignment of the 28 (i) and 31 (j) MHz resonances in the inhibited narrow singlet (Figure 4D) to methylene proton hyperfine coupling constants was achieved in conjunction with the parameters obtained from simulation of the EPR spectra. The proton hyperfine parameters obtained for the wide doublet and the inhibited narrow singlet are listed in Table 2. The EPR spectra that were calculated by using these parameters are shown in Figure 2A,B for comparison with the experimental wide-doublet and inhibited narrow-singlet spectra. The g values, obtained by simulation, are consistent with previously published results for tyrosyl radicals (*36*, *37*) and can be used to provide insight into the hydrogen-bonding status of the radicals, as discussed below (*38*−*41*). The agreement between the simulated spectra and the experimental data is good, despite the omission, in the simulations, of the smaller proton hyperfine couplings considered in the next section.

(C) Other Weakly Coupled Protons. The hyperfine tensor components of the 2,6-ring protons and the weakly coupled methylene proton are relatively small. Thus, the ENDOR signals from these protons will reside in the wings of the matrix proton signal in the 10−20 MHz region of the X-band spectra. The ENDOR spectra of the matrix proton region for the inhibited narrow-singlet and the wide-doublet species are shown in Figure 5. For the wide doublet (Figure 5B), three lines (b−d) are resolved in the FM-ENDOR spectrum in derivative mode. As mentioned above, the analogies in peak shape and frequency of these features to those of known tyrosyl radicals (*19*, *23*, *24*, *26*, *27*) make the assignment of these lines straightforward. The resultant tensor components, although not complete, are summarized in Table 2. The inhibited narrow-singlet ENDOR spectrum (Figure 5A) shows the same set of resonances (b−d), but, in addition, shows a fourth feature, a, which is apparent in the inset at 12.8 and 15.9 MHz and corresponds to a hyperfine coupling of 3.1 MHz. The amplitude of a was reduced, although not eliminated, in the ENDOR spectrum of PGHS in D_2O (Figure 5A, inset). This suggests that a arises from a hydrogen-bonded proton to the phenol headgroup of the tyrosyl radical in the inhibited enzyme (*42*, *43*). In contrast, the ENDOR spectrum of the wide-doublet radical shows no feature in this region and its spectrum is insensitive to D_2O exchange (Figure 5B, inset), indicating that the active form of the radical is unlikely to be hydrogen bonded.

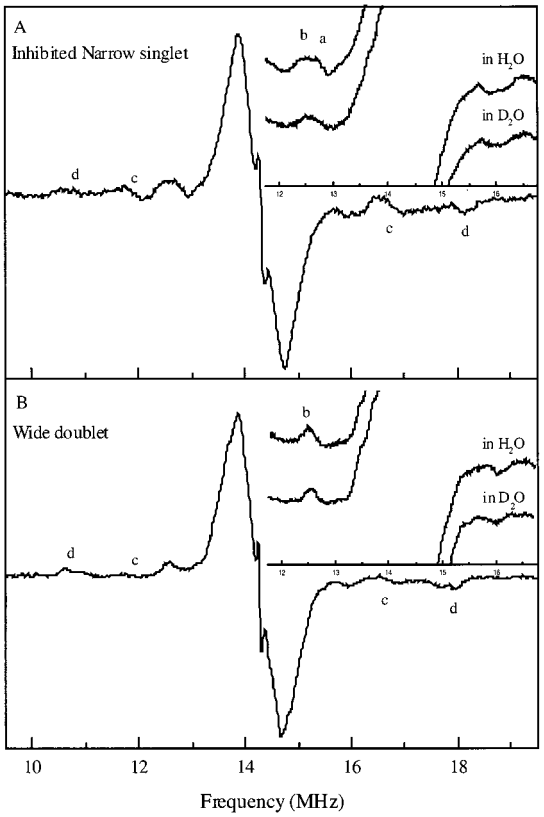

FIGURE 5: X-band, frequency-modulated-ENDOR spectra in the matrix proton region for PGHS-1 radicals. (A) Inhibited narrow-singlet tyrosyl radical. (B) Wide-doublet tyrosyl radical. Spectrometer conditions: microwave frequency = 9.4 GHz, microwave power = 2 mW, magnetic field = 3348 G, rf power = 80 W at 9.5 MHz, rf modulation = 60 kHz. Insets show higher-resolution ENDOR spectra obtained with lower rf modulation amplitude (rf power = 80 W at 11.75 MHz and rf modulation = 40 kHz).

(4) EPR Line Width Study. We have shown above that the PGHS-1 wide-singlet EPR signal does not reflect a distinct tyrosyl radical species and that this signal decays with time, ending up with a line shape similar to, but slightly wider than, the narrow singlet of indomethacin-treated enzyme. In this section, we present evidence that this reaction-inactivated 25-G narrow-singlet EPR signal represents a tyrosyl-radical species that is distinct from the inhibited 22-G narrow-singlet species.

Since the wide-singlet signal is a combination of the initial wide doublet and the final reaction-inactivated narrow singlet, as originally suggested by DeGray et al. (*9*) and confirmed by the ENDOR results above, arithmetic subtraction of the wide doublet from the wide singlet should give rise to the final narrow singlet. Subtractions of various fractions of the wide doublet (Figure 1A) from the wide singlet (Figure 1B) were tried, and the composite spectrum resulting from subtraction of 40% of the wide doublet (Figure 6A) was found to give the best agreement with the inactivated narrow singlet observed in the kinetic studies (Figures 6B and 1K). During these subtractions, the spectra were kept aligned at their g_y and g_z values, as high-frequency EPR spectroscopy has shown that these two g values are essentially constant among various tyrosyl radicals, whereas g_x changes significantly (*37*, *44*, *45*). A key point is that the composite spectrum A in Figure 6 has a line width of 25 G, identical to the final signal in the kinetic study (Figure 6B) and

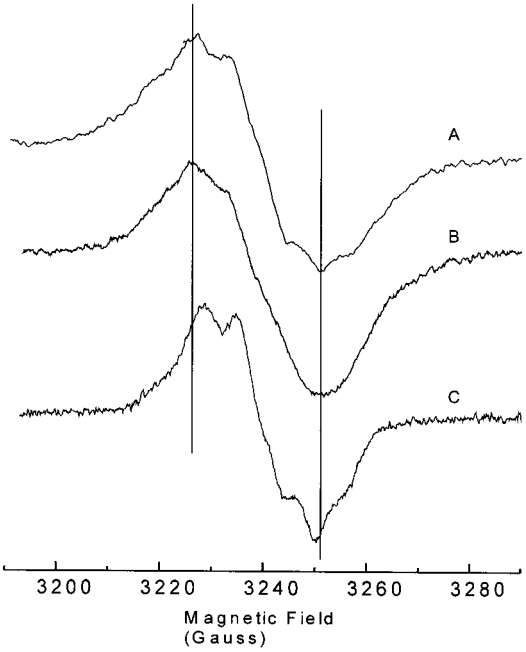

FIGURE 6: Arithmetic analysis of PGHS-1 EPR spectra. Spectrum A is the arithmetic composite that results when 40% of the wide doublet is subtracted from the wide singlet. Spectrum B is the experimentally observed, self-inactivated narrow singlet (Figure 1K). Spectrum C is the inhibited narrow singlet (Figure 1L). The vertical lines align the g_y and g_z components of all three spectra.

considerably broader than the narrow singlet observed in indomethacin-treated enzyme (~ 22 G) (Figure 6C).

In further arithmetic manipulation of the EPR spectra, we combined the wide-doublet signal with variable amounts of the inhibited narrow-singlet signal (~22 G). In all cases, the resultant was narrower than the observed wide-singlet signal (not shown). The combination that came closest to fitting the line shape of the observed wide singlet had equal portions of the wide doublet and the inhibited narrow singlet. However, even this optimal composite spectrum was about 3 G narrower than the experimental wide-singlet signal (Figure 1B). This implies that the narrow-singlet component of the observed wide-singlet signal has to be about 3 G broader than the 22-G signal observed for inhibited enzyme, or 25 G. There was no indication that the 25-G reaction-inactivated narrow-singlet signal could be further narrowed by extended reaction (Figure 1). We conclude, consequently, that the two narrow-singlet species arise from conformationally distinct tyrosyl radicals.

DISCUSSION

Several tyrosyl-radical signals of different line widths are detected during PGHS-1 reaction with hydroperoxide by conventional EPR, as shown in Figure 1. However, only the radical showing the wide doublet from reaction of the native enzyme with peroxide substrates and the radical from inhibited enzyme, showing a narrow singlet, have distinct conformations, as judged by the ENDOR signals that arise from the strongly coupled tyrosyl β-methylene protons. The ENDOR results show that wide-singlet-type EPR spectra result from a mixture of the initial, native wide-doublet species and the reaction-inactivated narrow-singlet species; they do not arise from distinct conformational entities.

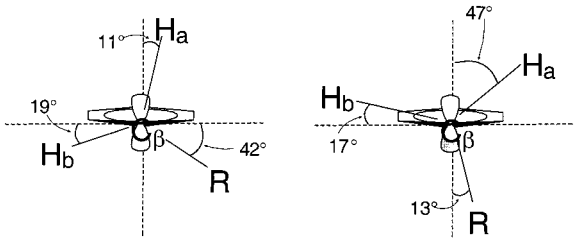

FIGURE 7: Conformations of the β-methylene group of the tyrosyl radical that gives rise to (left) the wide-doublet EPR spectrum and (right) the indomethacin-inhibited narrow-singlet spectrum, as determined from the ENDOR data. See text for details.

The conformation of the tyrosyl-radical methylene group with respect to the ring plane can be determined from the strength of the hyperfine coupling to the two methylene protons, H_a and H_b (Scheme 1). These couplings originate from through-bond interactions between these nuclei and the ring π-electron system and are dependent upon the spin density on ring carbon 1 (ρ_{C1}) and the dihedral angle θ (Scheme 1) for each proton, according to the modified McConnell relationship:

$$A_{iso} = \rho_{C1} (B_0 + B_2 \cos^2 \theta) \quad (2)$$

where B_0 and B_2 are constants. B_0 is close to zero, and the value of B_2 appropriate for alkyl radicals is ~162 MHz (*46*); Bender et al. (*19*) derived similar values for these two parameters for the tyrosyl radical in ribonucleotide reductase. For the wide doublet in PGHS-1, we observe only a single, strongly coupled methylene proton (A_{iso} = 59.3 MHz), so an independent assessment of ρ_{C1} is not yet possible. However, detailed analysis of radical spin densities in both model and enzyme systems shows that the spin-density distribution for tyrosyl radicals is almost invariant (*23*). Therefore, we assume for PGHS a ρ_{C1} of 0.38 and a B_2 value of 162.4 MHz (*19*) and obtain a θ value of 11° for the $C_\beta-H_a$ bond in the wide-doublet conformation. With this dihedral angle for $C_\beta-H_a$, and assuming that the two $C_\beta-H$ bonds and the $C_\beta-R$ bond are related by 120° rotations, characteristic of sp^3 hybridization, two geometries for H_b and the R group are possible. In one, the dihedral angles for $C_\beta-H_b$ and $C_\beta-R$ are 71° and 49°, respectively. In the second, these two dihedral angles are reversed, i.e., 49° for $C_\beta-H_b$ and 71° for $C_\beta-R$. The second of these two geometries predicts a significant hyperfine coupling to the $C_\beta-H_b$ proton, 27 MHz, which we do not detect in the ENDOR nor require in the simulations in Figure 2. Thus, we conclude that the second geometry is unlikely and that the orientation of H_a, H_b, and R around C_β in Figure 7 (left) is more consistent with our data.

For the inhibited narrow-singlet conformation, we detect a methylene proton coupling with A_{iso} of about 29 MHz. Analysis within the context of eq 2 yields a dihedral angle of 47° for $C_\beta-H_a$. As with the wide doublet, there are no indications of a second, relatively large, β-methylene proton coupling and, accordingly, we conclude that the geometry shown in Figure 7 (right) describes the orientation about C_β in the inhibited, narrow singlet conformation. As noted above, however, the β protons in the inhibited narrow singlet have ENDOR line shapes indicative of dispersion in their dihedral angles (*31*). Figure 7 (right) thus presents only the average orientation of the methylene group with respect to the phenol ring.

Tyrosine residues are functionally important, redox-active cofactors in a number of enzymes (*26, 35, 47*−*64*). Although the protein environments around the tyrosines are quite different in these enzymes, the EPR signals of their radical forms fall into two major categories. The first is characterized by a wide-doublet-type EPR spectrum, with a peak-to-trough width of about 33 G; representatives include ribonucleotide reductase, galactose oxidase, the wide-doublet species that occurs at early times following peroxide reaction in PGHS, and, possibly, the recently uncovered wide-doublet species in linoleate diol synthase. The second category is characterized by a narrower line shape, with a peak-to-trough width of about 24 G. Representative species in this class include $Y_D^\bullet$ and $Y_Z^\bullet$ in photosystem II, model tyrosine radicals in alkaline glasses (*31, 64*), the tyrosyl radical in *Salmonella typhimurium* ribonucleotide reductase (*51*), and the inhibitor-induced and reaction-inactivated tyrosyl radicals in PGHS. PGHS is the only protein found, so far, where both types of tyrosyl-radical species are evident.

The radicals in these two general conformational classes differ in their side-chain energetics. From magnetic-resonance work with tyrosyl radicals in solution, Sealy et al. (*65*) estimated that the rotational barrier between different conformations about the C1−Cβ bond can be as high as 10 kcal/mol. Using a computational approach, we performed semiempirical AM1 calculations on tyrosine in the gas phase and found the rotational barrier to be about 3 kcal/mol (unpublished data; see, also, refs *66* and *67*). In these calculations, the narrow singlet corresponds to the lower-energy conformation; the wide-doublet conformation lies near the top of the energy barrier. In more rigorous calculations, Qin and Wheeler (*68*), O'Malley and Ellson (*69*), and Himo et al. (*25*) have applied density-functional methods to tyrosyl radicals. In the latter work, which involved the gas-phase radical, a rotational barrier of ~1 kcal was observed. Interestingly, the rotational surface has a local minimum near the geometry we predict for the wide-doublet conformation (Figure 7, left) and a global minimum at the geometry deduced for the narrow singlet (Figure 7, right). Thus, we conclude that high-energy conformations of enzymatically active tyrosyl radicals are found in protein systems, which indicates that these tyrosyl species are subjected to steric constraints imposed by the protein. Moreover, the fact that the loss of the high-energy conformation accompanies self-inactivation in PGHS-1 implicates the maintenance of conformational fidelity in enzyme function. The computational work cited above is consistent in demonstrating that rotation about the C1−C$_\beta$ bond has no observable effect on the electronic properties of the radical nor on its spin-density distribution. Thus, we can eliminate such factors in considering conformation control of radical reactivity, which suggests that the geometry of the tyrosyl oxygen lone pairs is the physical property that the ring conformation is designed to preserve. Consistent with this, Ingold and coworkers (*70*) have implicated the spatial orientation of the oxygen lone pairs relative to the hydrogen atom in an abstraction process as an important factor in determining the overall reaction efficiency.

These considerations, and the tyrosyl geometries deduced in Figure 7, suggest that a plausible rationale for enzyme

inhibition upon self-inactivation or inhibitor binding involves perturbations to the active conformation of the catalytically essential Y385 residue. The mutagenesis work shows clearly that the functionally relevant, wide-doublet species is uniquely associated with a native Y385 site (*11*). The alternative, however, that the location of the radical switches from Y385 in the wide-doublet species to other tyrosines in the inhibited or self-inactivated protein requires consideration. This is especially so because tyrosyl radicals in ribonucleotide reductase (*71*, *72*) and in other radical-enzyme systems (*35*) have been shown to migrate and locate at alternate sites under certain circumstances. There is evidence that similar alternate-site phenomena occur in PGHS. In Y385F mutants, cyclooxygenase activity is lost, and the wide-doublet signal is replaced by a narrow singlet that is essentially identical to the signal observed when the enzyme is inhibited with indomethacin (*11*). This result indicates that while Y385 is necessary for cyclooxygenase activity, it is not required to produce the 22-G, narrow-singlet signal. Moreover, the spectral similarities between the singlets observed in the Y385F mutant and indomethacin-inhibited PGHS-1 suggest that indomethacin inhibits PGHS by redirecting radical formation to a side chain other than Y385. The nearly identical microwave power saturation behavior of the wide doublet and the narrow singlets (*10*, *11*) indicates that these species have very similar magnetic environments. The X-ray structure (*73*) reveals several tyrosine residues in the vicinity of the PGHS-1 heme that are candidates for the alternative tyrosine-radical site in the Y385F mutant. A further mutagenic study to identify the tyrosyl residue responsible for the narrow-singlet signal, however, was not conclusive (*74*).

The origin of the narrow singlet that occurs upon self-inactivation is more obscure, as we were unable to record ENDOR spectra for this species owing to its diminished concentration. Thus, both inhibitory mechanisms, radical repositioning and conformational relaxation, remain plausible for this species. Additional experiments will be necessary to resolve this issue and the implications it has for suicide inactivation in PGHS.

Our ENDOR experiments with the narrow-singlet species in the indomethacin-inhibited enzyme have also shown evidence of H/D isotopic exchange, implying hydrogen bonding to the phenoxyl oxygen. The hyperfine coupling constant of this exchangeable proton, 3.1 MHz, is within the range observed for other hydrogen-bonded tyrosyl radicals (*30*, *75*, *76*). The isotopic exchange rate for the PGHS-1 narrow-singlet species is slow—even after overnight incubation at 8 °C, there was still some 15.9 (and 12.8) MHz intensity (Figure 5) remaining in the D_2O-treated sample, reflecting incomplete exchange. Such slow D_2O exchange kinetics have also been reported for $Y_D^{\bullet}$ in photosystem II (*75*−*77*). Features attributable to a hydrogen-bonding interaction and H/D isotopic exchange effects, however, were not observed in the ENDOR spectrum of the wide-doublet species generated in the reaction of native PGHS, indicating that the phenolic oxygen is not hydrogen bonded in this species, despite its proximity to the phenolic hydrogen on Y348 in the PGHS-1 crystal structure (*73*). The g_x values required to simulate the wide-doublet and inhibited narrow-singlet spectra (Table 1) support this analysis. The 2.0089 g_x value for the wide doublet is consistent with a non-hydrogen-bonded phenol oxygen. The lower value, 2.0074, for the inhibited narrow-singlet suggest that the tyrosine that gives rise to this spectrum is hydrogen-bonded (*37*, *38*, *40*, *41*).

Lack of hydrogen bonding to the phenolic oxygen of the wide-doublet tyrosyl radical may have important functional implications for catalysis by PGHS. Considerable experimental evidence indicates that the cyclooxygenase reaction starts with removal of the *pro-S* hydrogen atom of the fatty acid to produce a carbon-centered radical that attacks O_2 to form a cyclic endoperoxide intermediate (*2*). The wide doublet accumulates in parallel with cyclooxygenase product and is, thus, kinetically competent for catalysis (*5*, *6*, *9*−*11*, *78*). The reactivity of a tyrosyl radical in abstracting hydrogen atoms from substrate is a function of the orientation of the donor/acceptor pair, as noted above, and the approach of the substrate and Y385, in its wide-doublet conformation, is likely to be facilitated by the absence of a hydrogen-bond donor and its associated steric bulk. These considerations also likely have relevance for hydrogen-atom abstraction mechanisms in myeloperoxidase (*79*) and in linoleate diol synthase (*59*).

To summarize, the magnetic-resonance data presented here provide new information on the hyperfine tensors and *g*-values for the tyrosyl radicals that occur in PGHS-1. These results indicate that there are two distinct narrow-singlet radical species. Moreover, we can conclude that the wide-singlet EPR is a sum of the wide doublet and the reaction-inactivated narrow singlet. With these ambiguities resolved, the complexity of tyrosyl radicals present in PGHS-1 is reduced, and attention can now be focused on the precise roles that these radicals play in catalysis and self-inactivation.

REFERENCES

1. Smith, W. L., Eling, T. E., Kulmacz, R. J., Marnett, L. J., and Tsai, A.-L. (1992) *Biochemistry 31*, 3.
2. Smith, W. L., Garavito, R. M., and DeWitt, D. L. (1996) *J. Biol. Chem. 271*, 33157.
3. Hamberg, M., and Samuelsson, B. (1967) *J. Biol. Chem. 242*, 5336.
4. Mason, R. P., Kalyanaraman, B., Tainer, B. E., and Eling, T. E. (1980) *J. Biol. Chem. 255*, 5019.
5. Tsai, A.-L., Kulmacz, R. J., and Palmer, G. (1995) *J. Biol. Chem. 270*, 10503.
6. Tsai, A.-L., Palmer, G., Xiao, G., Swinney, D. C., and Kulmacz, R. J. (1998) *J. Biol. Chem. 273*, 3888.
7. (a) Kulmacz, R. J., and Lands, W. E. M. (1987) in *Prostaglandins and Related Substances: A Practical Approach* (Benedetto, C., McDonald-Gibson, R. G., Nigam, S., and Slater, T. F., Eds.) p 209, IRL, Washington, DC. (b) Kulmacz, R. J., Tsai, A.-L., and Palmer, G. (1987) *J. Biol. Chem. 262*, 10524.
8. Karthein, R., Dietz, R., Nastainczyk, W., and Ruf, H. H. (1988) *Eur. J. Biochem. 171*, 313.
9. DeGray, J. A., Lassmann, G., Curtis, J. F., Kennedy, T. A., Marnett, L. J., Eling, T. E., and Mason, R. P. (1992) *J. Biol. Chem. 267*, 23583.
10. Kulmacz, R. J., Ren, Y., Tsai, A.-L., and Palmer, G. (1990) *Biochemistry 29*, 8760.
11. Tsai, A.-L., Hsi, L. C., Kulmacz, R. J., Palmer, G., and Smith, W. L. (1994) *J. Biol. Chem. 269*, 5085.
12. Hsi, L. C., Hoganson, C. W., Babcock, G. T., and Smith, W. L. (1994) *Biochem. Biophys. Res. Commun. 202*, 1592.
13. Xiao, G., Tsai, A.-L., Palmer, G., Boyar, W. C., Marshall, P. J., and Kulmacz, R. J. (1997) *Biochemistry 36*, 1836.
14. Gunther, M. R., Hsi, L. C., Curtis, J. F., Gierse, J. K., Marnett, L. J., Eling, T. E., and Mason, R. P. (1997) *J. Biol. Chem. 272*, 17086.

15. Shimokawa, T., Kulmacz, R. J., Dewitt, D. L., and Smith, W. L. (1990) *J. Biol. Chem. 265*, 20073.
16. Lassman, G., Odenwaller, R., Curtis, J. F., DeGray, J. A., Mason, R. P., Marnett, L. J., and Eling, T. E. (1991) *J. Biol. Chem. 266*, 20045.
17. Tsai, A.-L., Palmer, G., and Kulmacz, R. J. (1992) *J. Biol. Chem. 262*, 10524.
18. Hurst, G., Kraft, K., Shultz, R., and Kreilick, R. (1982) *J. Magn. Reson. 49*, 159.
19. Bender, C. J., Sahlin, M., Babcock, G. T., Barry, B. A., Chandrashekar, T. K., Salowe, S. P., Stubbe, J., Lindstrom, B., Petersson, L., Ehrenberg, A., and Sjoberg, B.-M. (1989) *J. Am. Chem. Soc. 111*, 8076.
20. Hoganson, C. W., and Babcock, G. T. (1995) *J. Magn. Reson., Ser. A 112*, 220.
21. Scholes, C. P. (1979) in *Multiple Electron Resonance Spectroscopy* (Dorio, M. M., and Freed, J. H., Eds.) p 297, Plenum Press, New York.
22. Gurbiel, R. J., Batie, C. J., Sivaraja, M., True, A. E., Fee, J. A., Hoffman, B. M., and Ballou, D. P. (1989) *Biochemistry 28*, 2861.
23. Babcock, G. T., Espe, M., Hoganson, C. W., Lydakis-Simantiris, N., McCracken, J., Shi, W., Styring, S., Tommos, C., and Warncke, K. (1997) *Acta Chem. Scand. 51*, 533.
24. Hoganson, C. W., and Babcock, G. T. (1992) *Biochemistry 31*, 11874.
25. Himo, F., Gräslund, A., and Eriksson, L. A. (1997) *Biophys. J. 72*, 1556.
26. Babcock, G. T., El-Deeb, M. K., Sandusky, P. O., Wittaker, M. M., and Wittaker, J. W. (1992) *J. Am. Chem. Soc. 114*, 3727.
27. Rigby, S. E. J., Nugent, J. H. A., and O'Malley, P. J. (1994) *Biochemistry 33*, 17334.
28. Atherton, N. M. (1993) *Principles of Electron Spin Resonance*, Ellis Horwood & Prentice Hall, New York.
29. Tommos, C., Tang, X.-S., Warncke, K., Hoganson, C. W., Styring, S., McCracken, J., Diner, B. A., and Babcock, G. T. (1995) *J. Am. Chem. Soc. 117*, 10325.
30. Warncke, K., McCracken, J., and Babcock, G. T. (1994) *J. Am. Chem. Soc. 116*, 7332.
31. Warncke, K., and McCracken, J. (1995) *J. Phys. Chem. 103*, 6829.
32. Warncke, K., Babcock, G. T., and McCracken, J. (1996) *J. Phys. Chem. 100*, 4654.
33. Hoganson, C. W., Sahlin, M., Sjöberg, B.-M., and Babcock, G. T. (1996) *J. Am. Chem. Soc. 118*, 4672.
34. Dole, F., Diner, B. A., Hoganson, C. W., Babcock, G. T., and Britt, R. D. (1997) *J. Am. Chem. Soc. 119*, 11540.
35. Stubbe, J., and van der Donk, W. A. (1998) *Chem. Rev. 98*, 705.
36. Gulin, V. I., Dikanov, S. A., Tsvetko, Y., Evelo, R. G., and Hoff, A. J. (1992) *J. Pure Appl. Chem. 64*, 903.
37. Gerfen, G. J., Bellew, B. F., Un, S., Bollinger, J. M., Jr., Stubbe, J., Griffin, R. G., and Singel, D. J. (1993) *J. Am. Chem. Soc. 115*, 6420.
38. Un, S., Tang, X. S., and Diner, B. A. (1996) *Biochemistry 35*, 679.
39. Elleingand, E., Gerez, C., Un, S., Knupling, M., Lu, G., Salem, J., Rubin, H., Sauge-Merle, S., Laulhere, J. P., and Fontecave, M. (1998) *Eur. J. Biochem. 258*, 485.
40. Ivancich, A., Mattiola, T. A., and Un, S. (1999) *J. Am. Chem. Soc. 121*, 5743.
41. Burghaus, O., Plato, M., Rohrer, M., Möbius, K., MacMillan, F., and Lubitz, W. (1993) *J. Phys Chem. 97*, 7639.
42. O'Malley, P. J., and Babcock, G. T. (1986) *J. Am. Chem. Soc. 108*, 3995.
43. Campbell, K. A., Peloquin, J. M., Diner, B. A., Tang, X.-S., Chisholm, D. A., and Britt, D. R. (1997) *J. Am Chem. Soc. 119*, 4787.
44. Un, S., Brunel, L.-C., Brill, T. M., Zimmermann, J.-L., and Rutherford, A. W. (1994) *Proc. Natl. Acad. Sci. U.S.A. 91*, 5262.
45. Un. S., Atta, M., Fontecave, M., and Rutherford, A. W. (1995) *J. Am. Chem. Soc. 117*, 10713.
46. Fessenden, R. W., and Schuler, R. H. (1963) *J. Chem. Phys. 39*, 2149.
47. Reichard, P., and Ehrenberg, A. (1983) *Science 221*, 514.
48. Larsson, A., and Sjöberg, B.-M. (1986) *EMBO J. 5*, 2037.
49. Sahlin, M., Petersson, L., Graslund, A., Ehrenberg, A., Sjoberg, B.-M., and Thelander, L. (1987) *Biochemistry 26*, 5541.
50. Stubbe, J. (1988) *Biochemistry 27*, 3893.
51. Allard, P., Barra, A. L., Andersson, K. K., Schmidt, P. P., Atta, M., and Gräslund, A. (1996) *J. Am. Chem. Soc. 118*, 895.
52. Whittaker, M. M., and Whittaker, J. W. (1988) *J. Biol. Chem. 263*, 6074.
53. Whittaker, M. M., and Whittaker, J. W. (1990) *J. Biol. Chem. 265*, 9610.
54. Whittaker, M. M., Devito, V. L., Asher, S. A., and Whittaker, J. W. (1989) *J. Biol. Chem. 264*, 7104.
55. Baron, A. J., Stevens, C., Wilmot, C., Seneviratne, K. D., Blakeley, V., Dooley, D. M., Phillips, S. E. V., Knowles, P. F., and McPherson, M. J. (1994) *J. Biol. Chem. 269*, 25095.
56. Jones, S. M., Mu, D., Wemmes, D., Smith, A. J., Kaus, S., Maltby, D., Burlingame, A. L., and Kinman, J. P. (1990) *Science 248*, 981.
57. Ivancich, A., Jouve, H. M., and Gaillard, J. (1996) *J. Am. Chem. Soc. 118*, 12852.
58. Ivancich, A., Jouve, H. M., Sartor, B., and Gaillard, J. (1997) *Biochemistry 36*, 9356.
59. Su, C., Sahlin, M., and Oliw, E. H. (1998) *J. Biol. Chem. 273*, 20744.
60. Barry, B. A., and Babcock, G. T. (1987) *Proc. Natl. Acad. Sci. U.S.A. 84*, 7099.
61. Debus, R. J., Barry, B. A., Babcock, G. T., and McIntosh, L. (1988) *Proc. Natl. Acad. Sci. U.S.A. 85*, 427.
62. Debus, R. J., Barry, B. A., Sithole, I., Babcock, G. T., and McIntosh, L. (1988) *Biochemistry 27*, 9071.
63. Vermass, W. F. J., Rutherford, A. W., and Hansson, O. (1988) *Proc. Natl. Acad. Sci. U.S.A. 85*, 8477.
64. Barry, B. A., El-Deeb, M. K., Sandusky, P. O., and Babcock, G. T. (1990) *J. Biol. Chem. 265*, 20139.
65. Sealy, R. C., Harman, L., West, P. R., and Mason, R. P. (1985) *J. Am. Chem. Soc. 107*, 3401.
66. O'Malley, P. J., and MacFarlane, A. J. (1992) *J. Mol. Struct. (Theor. Chem.) 277*, 293.
67. O'Malley, P. J., MacFarlane, A. J., Rigby, S. E. J., and Nugent, J. H. A. (1995) *Biochim. Biophys. Acta 1232*, 175.
68. Qin, Y., and Wheeler, R. A. (1995) *J. Am. Chem. Soc. 117*, 6083.
69. O'Malley, P. J., and Ellson, D. (1997) *Biochim. Biophys. Acta 1320*, 65.
70. Foti, M., Ingold, K. U., and Lusztyk, J. (1994) *J. Am. Chem. Soc. 116*, 9440.
71. Gräslund, A., and Sahlin, M. (1996) *Annu. Rev. Biophys. Biomol. Struct. 25*, 259.
72. Logan, D. T., Andersson, J., Sjoberg, B. M., and Nordlund, P. (1999) *Science 283*, 1499.
73. Picot, D., Loll, P. J., and Garavito, R. M. (1994) *Nature 367*, 243.
74. Hsi, L. C., Hoganson, C. W., Babcock, G. T., Garavito, R. M., and Smith, W. L. (1995) *Biochem. Biophys. Res. Commun. 207*, 652.
75. Rodriguez, I. D., Chandrashekar, T. K., and Babcock, G. T. (1987) in *Progress in Photosynthesis Research* (Biggins, J., Ed.) p 471, Martinus Nijhoff, Dordrecht, The Netherlands.
76. Tang, X.-S., Chisholm, D. A., Dismukes, G. C., Brudvig, G. W., and Diner, B. A. (1993) *Biochemistry 32*, 13742.
77. Evelo, R. G., Hoff, A. J., Dikanov, S. A., and Tyryshkin, A. M. (1989) *Chem. Phys. Lett. 161*, 479.
78. Tsai, A.-L., Wu, G., Palmer, G., Bambai, B., Koehn, J. A., Marshall, P. J., and Kulmacz, R. J. (2000) *J. Biol. Chem.* (in press).
79. Savenkova, M. I., Mueller, D. M., and Heinecke, J. W. (1994) *J. Biol. Chem. 269*, 20394.

BI992561C